Alternative Refrigerants R123a, R134, R141b, R142b, and R152a: Critical Temperature, Refractive Index, Surface Tension, and Estimates of Liquid, Vapor, and Critical Densities

Hee Baik Chae,† James W. Schmidt,* and Michael R. Moldover

Thermophysics Division, National Institute of Standards and Technology (formerly National Bureau of Standards), Gaithersburg, Maryland 20899 *(Received: May 4, 1990)*

Differential capillary rise and refractive index data are reported for five alternative refrigerants: R123a ($CHClF-CClF_2$), R134 (CHF_2-CHF_2), R141b (CCl_2F-CH_3), R142b ($ClCF_2-CH_3$), and R152a (CHF_2-CH_3). The data extend from about 25 °C to the critical point of each fluid and directly yield the critical temperature T_c and the temperature-dependent capillary length. The present data were combined with liquid density data (near ambient temperature) to determine the Lorentz–Lorenz constant. The Lorentz–Lorenz relation is used to estimate the liquid, vapor, and critical densities, and the surface tension. The surface tension σ of seven substituted ethane refrigerants [the present five and R123 ($CHCl_2-CF_3$) and R134a (CF_3-CH_2F)] is within ±10% of the expression: $\sigma = 64\ \mathrm{mN/m}\cdot t^{1.26}$, where $t = (T_c - T)/T_c$ is the reduced temperature measured from the critical temperature. The surface tension of the same seven refrigerants is within ±5% of the expression $\sigma = 5.7t^{1.26}k_BT_c(N_A/V_c)^{2/3}$, where k_B, N_A, and V_c are the Boltzmann constant, the Avogadro constant, and the molar critical volume, respectively. R141b slowly decomposed when maintained near its critical point (in contact with gold, sapphire, stainless steel, and crown glass).

I. Introduction

In the near future, the production of certain fully halogenated chlorofluorocarbon (CFC) compounds that are used as refrigerants, solvents, and foam blowing agents will be phased out. There are several promising fluids that may serve as subtitutes, either as pure fluids or as constituents of mixtures, or both. In previous publications[1,2] we reported differential capillary rise data for the leading candidates to replace R11 (CCl_3F) and R12 (CCl_2F_2), namely R123 ($CHCl_2-CF_3$) and R134a (CF_3-CFH_2), respectively. For these leading candidates, there was ample density data in the literature[2] to obtain the surface tension from the capillary rise. (In that work, the surface tension was measured to facilitate the prediction of heat transfer when phase changes occurred. The surface tension influences the nucleation of bubbles in evaporators and the drainage of condensate from condenser surfaces.)

In the present work, we consider five other alternative refrigerants. For these fluids, neither the surface tension nor the liquid and vapor densities were available at the time we started this work. Accordingly, we have measured the indices of refraction of the liquid and vapor phases in addition to the capillary rise. The data were combined with very limited measurements of liquid densities[3-6] and the Lorentz–Lorenz relation to estimate the liquid and vapor densities throughout the two-phase region as well as the critical density and the surface tension. Because the Lorentz–Lorenz relation is not exact, the estimated densities are subject to systematic errors; however, the density errors from this source are less than 1% of the density of the liquid refrigerants near their boiling points. In the present work, the critical temperatures T_c were determined precisely by the refractive index data themselves; thus, they were not subject to error from imperfections in the Lorentz–Lorenz relation.

The five refrigerants considered here are (1) R123a, which is a significant impurity in R123 as manufactured and used; (2) R134, which is a potential competitor to R134a as a replacement for R12; (3) R141b, which is a potential replacement for R11 in foam blowing applications; (4) R142b, which may be used in mixtures; and (5) R152a, which is a component of a commercially available ternary mixture that might become a "drop in" replacement for R12 in home refrigerators and automotive air conditioners.

* Author to whom correspondence should be addressed.
† Current address: Korea Standards Research Institute, Taejon, Korea.

II. Materials

The refrigerants used in this study were obtained from the various sources. R123a was obtained from Allied Signal Corp.[7] Samples of this refrigerant were analyzed by Karl Fisher titration and found to contain 17 ± 3 ppm H_2O. In addition, 0.91% R123 was found to be present by gas chromatography. (Compositions were measured in mole percent.)

R134 was commercially purchased from PCR Corp.[7] and used without further purification. The manufacturer stated that its purity was 99.4% and that the principal impurity was perfluorocyclobutane.

R141b was obtained from Pennwalt Co.[7] One sample of this refrigerant was found to contain 53 ± 13 ppm H_2O; a second contained 16 ppm H_2O. Trace amounts of other compounds totaling less than 0.05% were found and included R11 (0.001%), R142b (0.003%), R365 (0.023%), and R1130a (0.017%).

R142b was commercially purchased from Pennwalt Corp.[7] and used without further purification. The manufacturer stated that its purity was 99.97% and that the water content was 15 ppm. Other impurities were R141b (0.02%), R152a (0.004%), and R11.

R152a was obtained from the E. I. DuPont Co.[7] The manufacturer stated that its minimum purity was 99.97% and that the water content was typically 1 ppm and the R12 content was typically 10 ppm.

III. Apparatus and Procedures

A horizontal cross section of the experimental cell is shown in Figure 1. The cross section shows the four Pyrex glass capillary tubes that were used to measure the capillary length and the crown

(1) Chae, H. B.; Schmidt, J. W.; Moldover, M. R. *J. Chem. Eng. Data* **1990**, *35*, 6.
(2) McLinden, M. O.; Gallagher, J. S.; Weber, L. A.; Morrison, G.; Ward, D. K.; Goodwin, A. R. H.; Moldover, M. R.; Schmidt, J. W.; Chae, H. B.; Bruno, T. J.; Ely, J. F.; Huber, M. L. *ASHRAE Trans* **1989**, *95*, part II, 263.
(3) Morrison, G.; Ward, D. K. *Fluid Phase Equilib.*, in press.
(4) Mears, M. H.; Stahl, R. F.; Orfeo, S. L.; Schair, R. C.; Kells, L. F.; Thompson, W.; McCann, H. *Ind. Eng. Chem.* **1955**, *47*, 1449.
(5) Valtz, A.; Laugier, S.; Richon, R. *Int. J. Refrig.* **1986**, *9*, 282.
(6) Higashi, Y.; Ashizawa, M.; Kabata, Y.; Majima, Y.; Uematsu, M.; Watanabe, K. *Jpn. Soc. Mech. Eng. Int. J.* **1987**, *30*, 1106.
(7) In order to describe materials and experimental procedures adequately, it was occasionally necessary to identify commercial products by manufacturers' names or labels. In no instance does such identification imply endorsement by the National Institute of Standards and Technology, nor does it imply that the particular product or equipment is necessarily the best available for the purpose.

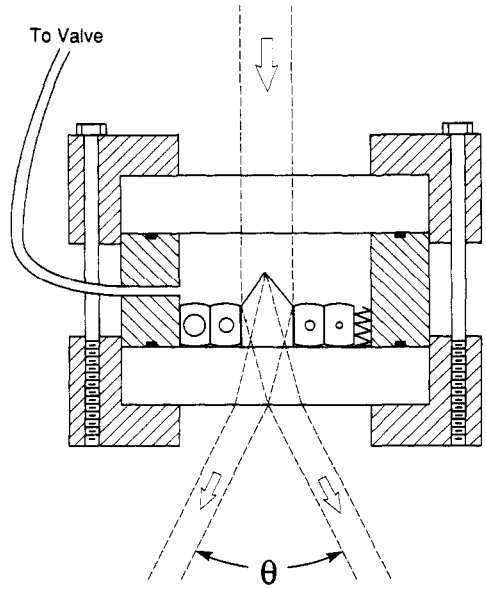

Figure 1. Horizontal cross section of the experimental cell showing four capillary tubes with sides ground flat and the prism that splits the laser beam for the refractive index measurements. The cylindrical body of the cell and the spring holding the capillaries are stainless steel; the windows are sapphire, and the O-ring is gold.

glass prism that was used to measure the indices of refraction of the liquid and vapor phases of each refrigerant.

The body of the experimental cell was a hollow, horizontal, stainless-steel cylinder 2.54 cm long. Sapphire windows, 3.07 cm in diameter and 0.63 cm thick were clamped to the ends of the cylinder by bolts and retaining rings that are not shown. Gold wire O-rings were used between the windows and the body of the cell. A short, 1/16 in. o.d. stainless steel tube had been welded to the body of the cell and led to a small stainless-steel valve that was used to retain the samples within the cell. Thus, while the refrigerant samples were hot, the only materials that they contacted were stainless steel, sapphire, gold, and glass.

Two flat surfaces were ground on each capillary to facilitate mounting it in the cell. The capillary tubes and the prism were retained in position by stainless-steel spring clips. The volume of the sample cell was approximately 6.5 cm^3.

The surface tension σ is related to the capillary length parameter a through

$$\sigma = a^2(\rho_l - \rho_v)g/2 \quad (1)$$

where ρ_l and ρ_v are the densities of the liquid and vapor, respectively, and g is the acceleration due to gravity 9.80 m/s^2. We have determined a with a differential capillary rise technique that avoids the difficult measurement of the height h_0 that a meniscus would have in a very wide cell. Instead, at each temperature, we measured the height differential Δh of the meniscii in two different capillaries with larger and smaller radii r_l and r_s, respectively.

The capillary length parameter a was determined from an iterative procedure described by Lane[8] that is claimed to be more accurate than the use of Sugden's tables.[9] Lane provides polynomial functions $f(r/a)$ which can be combined with a rough estimate of a to calculate the capillary rise h_l in the larger of two tubes without having measured the bulk meniscus level h_0:

$$h_l = (a_i^2/r_l)f(r_l/a_i) \quad (2)$$

h_l is then used to obtain a better estimate of a^2:

$$a_{i+1}^2 = r_s(\Delta h + h_l)f(r_s/a_i) \quad (3)$$

The procedure is iterated until the solution converges. This procedure assumes that the liquid–glass contact angle is zero. (It appeared to be so.)

The sample cell contained four capillaries with bore radii: $r_1 = 0.574 \pm 0.001$ mm, $r_2 = 0.320 \pm 0.001$ mm, $r_3 = 0.276 \pm 0.002$ mm, and $r_4 = 0.148 \pm 0.002$ mm. Those with the larger radii were used far from T_c; those with the smaller radii were used close to T_c. The meniscus heights h_i were measured to ± 0.01 mm by using a cathetometer. The radii of the capillaries were determined prior to their installation by partially filling them with plugs of mercury; the plugs were weighed and their lengths were measured with a traveling microscope. This procedure was repeated three times for each capillary.

The refractive index n_r of the refrigerant was deduced from measuring the angle θ between two beams of light that were refracted by the prism–refrigerant interface within the cell (see Figure 1). The working relation is

$$n_r = -\sin(\theta/2)\tan(\theta_p/2) + [n_p^2 - \sin^2(\theta/2)]^{1/2} \quad (4)$$

where $\theta_p = 90.027°$ is the angle of the prism that divided the light beam and $n_p = 1.5154 \pm 0.0001$ is the refractive index of the prism. The prism was illuminated with an expanded, collimated laser beam ($\lambda = 0.633$ μm). The prism and the illuminating beam were tall enough to extend through the liquid–vapor interface. Thus, four refracted beams emerged from the cell. Two were used to measure the refractive index of the liquid phase n_l and two were used to measure the refractive index of the vapor phase n_v. The angle θ was determined from measurements of the positions of the refracted beams where they emerged from the thermostated bath and where they struck a wall. A simple scale and the unaided eye were sufficient for this purpose. An accurate refractometer had been used to measure θ_p and n_p.

Prior to the final filling of the cell, it was flushed several times with the refrigerant under study. The cell was placed in a thermostated oil bath (± 0.02 K) with flat transparent windows. The bath's temperature was monitored with a calibrated platinum resistance thermometer. Typically, the bath's temperature was raised from ambient temperature in steps of 10 K. The bath and the cell came to thermal equilibrium within about 10 min; however, in most cases, an additional hour elapsed before the meniscus heights were measured. This allowed for the comparatively slow draining of the capillaries. The hour interval may not have been long enough near T_c, where the smallest capillaries were used and the slowest draining occurred.

The refractive index data and the capillary rise data are tabulated in Table IV.

IV. Analysis

The refractive index differences $(n_l - n_v)$ were fitted by the equation

$$n_l - n_v = 2\Delta n_0 t^{0.325}(1 + n_1 t^{0.5} + n_2 t) \quad (5)$$

where the reduced temperature measured from the critical temperature T_c is defined by

$$t \equiv (T_c - T)/T_c \quad (6)$$

The fit determined T_c, the refractive index amplitude Δn_0, and two additional parameters n_1 and n_2. The exponents 0.325 and 0.5 in eq 5 were obtained from theory and are believed to be asymptotically correct near T_c.[10] Their use with data that extend so far from T_c could be questioned; however, other functional forms were tried in place of eq 5 and no better fits were obtained. The refractive index averages $(n_l + n_v)/2$ were fitted by the equation

$$n_l + n_v = 2n_c(1 + n_d t) \quad (7)$$

Here n_c is the critical refractive index and n_d is the slope of the rectilinear diameter.

Figure 2 displays the capillary length data. The data for each refrigerant were fitted by the equation

$$a^2 = a_0^2 t^{0.935}(1 + a_1 t) \quad (8)$$

where a_0^2 and a_1 were the fitting parameters. The exponent 0.935

(8) Lane, J. E. *J. Colloid Int. Sci.* **1973**, *42*, 145.
(9) Sugden, S. *J. Chem. Soc.* **1921**, *119*, 1483.
(10) Sengers, J. V.; Levelt Sengers, J. M. H. *Annu. Rev. Phys. Chem.* **1986**, *37*, 189.

TABLE I: Summary of Measurements

refrigerant	T_c, K	Δn_0	n_1	n_2	n_c	n_d	a_0^2, mm^2	a_1	t_{max}
123a	461.6	0.2249	0.189	−0.256	1.1196	0.1151	6.13	−0.05	0.35
134	391.8	0.1721	0.361	−0.489	1.0942	0.0923	6.98	−0.03	0.25
141b	477.3	0.2379	0.309	−0.379	1.1300	0.1247	7.64	0.02	0.32
142b	410.3	0.2027	0.361	−0.435	1.1120	0.1106	7.50	−0.09	0.28
152a	386.3	0.1851	0.211	−0.264	1.0967	0.1061	9.49	−0.07	0.23

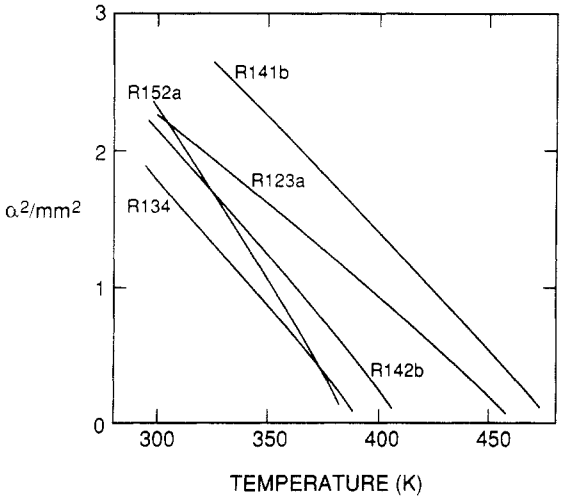

Figure 2. Capillary length parameter a^2 for five refrigerants.

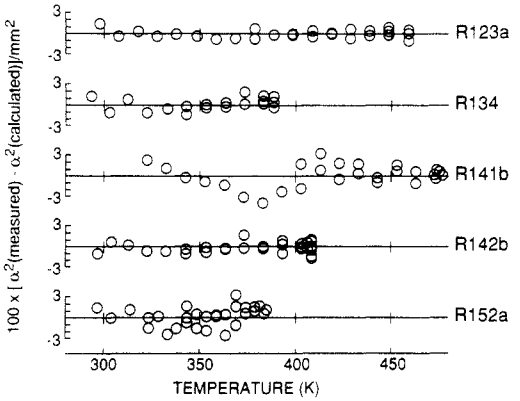

Figure 3. Deviations of the data for five refrigerants from eq 8, expressed as $\delta a^2 = a^2(\text{measured}) - a^2(\text{calculated})$. When several points appear at one temperature for a given refrigerant, they represent determinations of a^2 with different pairs of capillaries.

in eq 8 was taken from theory and is believed to be asymptotically correct near T_c[11] and T_c was taken from the refractive index difference fit. If T_c were allowed to vary while fitting eq 8 to the capillary length data, the resulting T_c's would have been 0.1–0.5 K higher than the T_c's obtained from the refractive index differences. We believe that T_c was determined more accurately by the refractive index differences because they were measured much closer to the critical point and because they are not subject to errors from trace impurities and/or bubbles in the capillary tubes or errors from the slow draining of the capillaries near T_c. The parameters resulting from the fitting are listed in Table I and the deviations of the data from the fitted equations are displayed in Figure 3. In Table I, the entries under the heading t_{max} indicate the greatest extent of the fitted data from T_c.

The refractive index data and the liquid density data at the isolated thermodynamic states listed in Table II were combined to determine the Lorentz–Lorenz "constant" k that appears in the relation

$$\frac{n^2 - 1}{n^2 + 2} = k\rho \qquad (9)$$

(11) Chaar, H.; Moldover, M. R.; Schmidt, J. W. *J. Chem. Phys.* **1986**, *85*, 418.

TABLE II: Reference Data for Estimating Densities

refrigerant	T, °C	ρ, kg/m^3	P, kPa	ref	MW, g/mol	k, cm^3/g
123a	30.02	1434	101	*a*	152.93	0.1408
134	25.02	1285	523	*a*	102.03	0.1149
141b	50.02	1177	185	*a*	116.95	0.1826
142b	25.00	1110	340	*b*	100.49	0.1621
152a	25.00	899	596	*c*	66.05	0.1705

[a] Morrison and Ward.[3] [b] McLinden (correlation of measurements from refs 4 and 5). [c] McLinden (correlation of measurements from ref 6).

TABLE III: Derived and/or Estimated Properties

refrigerant	$\Delta\rho_0/\rho_c$	ρ_1	ρ_2	ρ_c, kg/m^3	ρ_d	σ_0, mN/m	σ_1
123a	1.846	0.177	−0.314	550	0.892	63.6	−0.18
134	1.798	0.357	−0.539	535	0.921	70.3	−0.11
141b	1.783	0.307	−0.460	461	0.870	65.8	−0.09
142b	1.774	0.351	−0.493	449	0.911	62.9	−0.18
152a	1.881	0.222	−0.339	369	1.041	67.3	−0.13

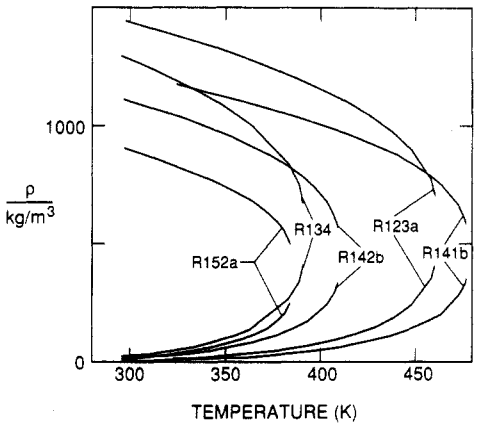

Figure 4. Density of five refrigerants estimated from the refractive index data via eq 9 and the Lorentz–Lorenz constants in Table II.

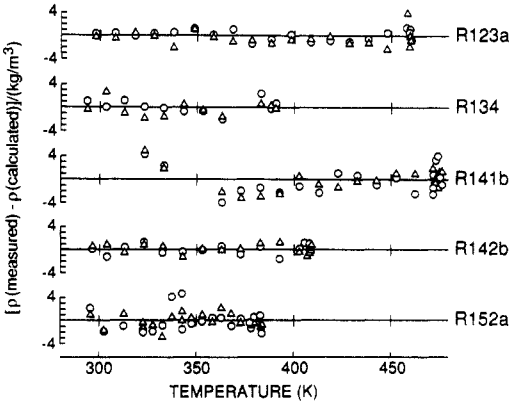

Figure 5. Deviations of the density data from eq 10 and 11, expressed as $\rho(\text{measured}) - \rho(\text{calculated})$. The triangles represent vapor-phase data; the circles represent liquid-phase data.

The resulting values of k for each refrigerant appear in Table II. Then, for each refrigerant, eq 9 was used to calculate liquid and vapor densities at other temperatures, up to the critical point. The

TABLE IV[a]

T/°C	a_{12}^2, mm^2	a_{23}^2, mm^2	a_{34}^2, mm^2	n_l	n_v	T/°C	a_{12}^2, mm^2	a_{23}^2, mm^2	a_{34}^2, mm^2	n_l	n_v
	Data for R123a						Data for R142b				
24.7	2.30			1.3291	1.0008	23.3	2.20			1.2887	1.0030
34.6	2.15			1.3233	1.0012	31.0	2.08			1.2836	1.0034
44.9	2.03			1.3176	1.0016	39.8	1.91			1.2770	1.0049
54.7	1.89			1.3115	1.0023	49.9	1.72			1.2699	1.0068
64.7	1.77			1.3046	1.0033	59.7	1.55			1.2621	1.0085
75.3	1.62			1.2984	1.0047	70.1	1.36	1.35		1.2527	1.0112
85.2	1.49			1.2913	1.0058	80.2	1.17	1.16		1.2438	1.0148
95.2	1.36			1.2839	1.0078	90.2	0.97	0.98		1.2336	1.0190
105.2	1.22	1.23		1.2763	1.0095	100.2	0.78	0.80		1.2224	1.0241
115.2	1.09	1.09		1.2680	1.0122	110.2	0.58	0.58		1.2095	1.0316
125.2	0.95	0.95		1.2595	1.0156	120.3	0.380	0.369	0.386	1.1933	1.0411
135.2	0.81	0.81		1.2501	1.0192	130.2	0.166	0.163	0.170	1.1699	1.0581
145.2	0.67	0.67		1.2398	1.0241	133.2	0.100	0.096	0.103	1.1588	1.0673
155.2	0.530	0.520		1.2278	1.0301	135.3	0.056	0.045	0.049	1.1479	1.0766
165.1	0.381	0.376	0.401	1.2140	1.0383	135.4	0.044	0.044	0.046	1.1473	1.0777
174.9	0.236	0.228	0.232	1.1964	1.0502	135.6	0.043	0.036	0.042	1.1454	1.0788
185.2	0.053	0.066	0.061	1.1667	1.0749	135.9	0.034	0.018	0.044	1.1438	1.0805
186.6				1.1576	1.0816	136.1	0.030	0.016	0.038	1.1420	1.0820
187.1				1.1540	1.0852						
187.3				1.1521	1.0868		Data for R152a				
						22.8	2.41			1.2440	1.0042
	Data for R134					30.1	2.22			1.2379	1.0042
20.3	1.91			1.2356	1.0032	40.1	1.99			1.2311	1.0062
29.7	1.72			1.2304	1.0041	50.2	1.71			1.2222	1.0083
39.4	1.57			1.2234	1.0058	50.3	1.72			1.2224	1.0083
49.7	1.36			1.2160	1.0077	55.0	1.60			1.2181	1.0095
59.9	1.17			1.2083	1.0103	60.1	1.45			1.2130	1.0113
70.2	0.97	0.98		1.2001	1.0136	64.8	1.33			1.2094	1.0142
80.2	0.80	0.79		1.1905	1.0179	69.9	1.23			1.2046	1.0164
90.3	0.602	0.597		1.1793	1.0234	70.2	1.21	1.20		1.2040	1.0149
110.2	0.208	0.199	0.196	1.1482	1.0451	75.1	1.09	1.07		1.1989	1.0175
115.3	0.087	0.094	0.081	1.1329	1.0570	80.4	0.94	0.92		1.1930	1.0204
117.9				1.1171	1.0713	85.2	0.81	0.82		1.1869	1.0234
						90.3	0.65	0.68		1.1806	1.0273
	Data for R141b					95.4	0.55	0.524	0.567	1.1727	1.0315
49.9	2.70			1.3498	1.0029	100.3		0.401	0.419	1.1634	1.0375
60.0	2.53			1.3426	1.0029	105.3		0.261	0.266	1.1524	1.0452
70.1	2.35					107.8			0.193	1.1452	1.0510
90.0	2.01			1.3212	1.0043	110.3			0.103	1.1350	1.0595
100.0	1.82			1.3136	1.0065	111.4			0.075	1.1293	1.0639
110.0	1.65			1.3059	1.0086						
120.0	1.50			1.2979	1.0107						
130.0	1.33	1.37		1.2902	1.0139						
140.0	1.19	1.21		1.2805	1.0172						
149.7	1.00	1.02		1.2705	1.0222						
159.7	0.84	0.85		1.2596	1.0272						
169.6	0.65	0.66		1.2472	1.0334						
179.6		0.486	0.494	1.2328	1.0425						
189.5		0.286	0.303	1.2144	1.0539						
199.0			0.120	1.1879	1.0747						
199.2			0.113	1.1863	1.0750						
199.7			0.098	1.1843	1.0777						
200.2			0.097	1.1820	1.0807						
201.1			0.070	1.1769	1.0848						
202.2			0.053	1.1709	1.0897						
203.2			0.028	1.1624	1.0973						

[a] The subscripts in the headings for the capillary length data denote the pair of capillary tubes used for the determination, with 1 referring to the largest tube and 4 to the smallest.

curves on Figure 4 are drawn through the calculated densities.

The calculated densities were fitted by the equations

$$\rho_l - \rho_v = 2\Delta\rho_0 t^{0.325}(1 + \rho_1 t^{0.5} + \rho_2 t) \quad (10)$$

$$\rho_l + \rho_v = 2\rho_c(1 + \rho_d t) \quad (11)$$

in close analogy with eqs 6–8. In eq 10, the fitting parameters were $\Delta\rho_0$ (the density difference amplitude), ρ_1, ρ_2, and implicitly T_c. In eq 11 the fitting parameters were ρ_c (the critical density) and ρ_d. The values of the fitting parameters are listed in Table III and Figure 5 displays the deviations of the densities from the fitting eqs 10 and 11.

Finally, eq 1 was used to calculate the surface tensions from the fitted parameters for the capillary constants and the density differences. The resulting representation of the surface tension has five numerical parameters in addition to T_c. To obtain a simpler two-parameter representation, the surface tensions were also fitted with the function

$$\sigma = \sigma_0 t^{1.26}(1 + \sigma_1 t) \quad (12)$$

In the range of the data, the two-parameter function, eq 12, is within 1.5% of the five-parameter function obtained by combining eq 1, 8, and 10. Because the systematic errors in the capillary length and density differences are each on the order of 2%, eq 12 represents the data within their accuracy. The results for the density differences and the surface tensions appear in Table III.

Upon inspection of Table III, it is clear that the surface tension parameters in eq 12 do not differ greatly from one another. If the surface tension data for R123 ($CHCl_2$–CF_3) and R134a (CF_3–CH_2F) that appear in Table III of ref 1 were analyzed with

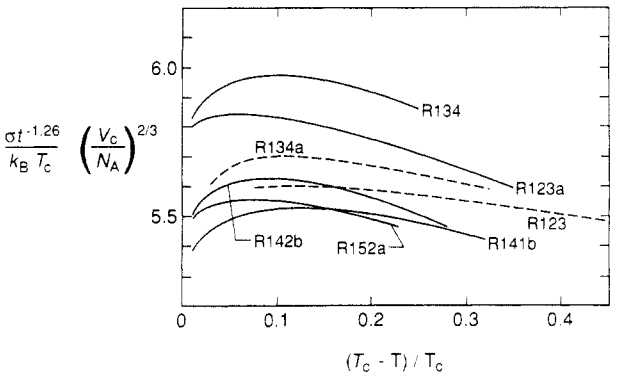

Figure 6. Scaled surface tension as a function of the reduced temperature for seven refrigerants. All the data fall within ±5% of the value 5.7. The solid curves are calculated from eqs 1, 8, and 10, using the parameters in Tables I and II. The dashed curves are taken from ref 1.

eq 12, the parameters would fall within the range spanned by those in Table III. Indeed the surface tension results for all seven substituted ethanes fall within ±10% of the expression

$$\sigma = 64 \text{ mN/m} \cdot [(T_c - T)/T_c]^{1.26}$$

The principle of corresponding states implies that it is useful to consider a reduced surface tension S that has been made dimensionless by the appropriate combination of critical parameters. The reduced surface tension for all seven substituted ethanes fall within ±5% of the expression

$$S = \frac{\sigma}{k_B T_c}\left(\frac{\text{MW}}{N_A \rho_c}\right)^{2/3} = 5.7 t^{1.26} \qquad (13)$$

(Here MW is the molecular weight, k_B is the Boltzmann constant, N_A is the Avogadro constant, and MW/ρ_c is the critical volume per mole, V_c.) The reduced surface tension S for seven refrigerents is shown in Figure 6. The refrigerants considered in Figure 6 differ greatly in chemical constituents, polarity, etc. Nevertheless the data nearly overlap. Thus we recommend the use of eq 13 for estimating the surface tension of other substituted ethanes and we anticipate errors on the order of ±5% for reduced temperatures in the range $0.01 \le t \le 0.35$. Equation 13 agrees with the surface tension of ethane itself at $t \approx 0.05$; however, it overestimates the surface tension of ethane by about 10% at the reduced temperature $t \approx 0.4$.[12]

V. Random and Systematic Errors

The standard deviation of the refractive index measurements was roughly 4×10^{-4}; however, discontinuities as large as 0.001 appear in the data and lead to discontinuities in the densities on the order of 0.003 gm/cm^3. The discontinuities resulted from errors in the measurements of angle θ which probably were caused by small displacements of the cell or the oil bath between measurements.

The standard deviation of the fits of eq 8 to the capillary length data ranged from 5×10^{-5} mm^2 for R123a to 16×10^{-5} mm^2 for R141b, the worst case. For R141b, the deviations from the fit (Figure 3) show a systematic trend with temperture and the values of a^2 determined from capillaries 2 and 3 were consistently larger (by as much as 3×10^{-4} mm^2 or 2.5% of a^2) than that determined from capillaries 1 and 2. One can speculate that these effects are related to the onset of decomposition of the sample (see section VII).

If the contact angles between one of the refrigerants and the capillary tubes were some small angle φ instead of zero, the true capillary length and surface tension for that refrigerant would have been larger than that reported here by a factor of $1/\cos(\varphi)$.

We now consider the errors resulting from the use of the Lorentz–Lorenz relation eq 10 to calculate the liquid and vapor densities from the refractive index data. To do so, we reviewed data for three fluids, H_2O, GeH_4, and SF_6, for which both density and refractive index data exist.[13-15] For each of these fluids, as for the refrigerants above, the Lorentz–Lorenz "constant" k was computed from measurements of the liquid density and the refractive index near the normal boiling point (NBP). Then the densities of the liquid and vapor were computed along the liquid–vapor coexistence curve ignoring any possible temperature and/or density dependence of k. Finally the computed densities were compared with the measured densities ρ_{meas}. The density error

$$\delta\rho = \rho_{meas} - \frac{1}{k}\frac{n^2 - 1}{n^2 + 2} \qquad (14)$$

is zero for the liquid at the calibration point and for the dilute vapor where ρ_{meas} approaches zero and n approaches 1. For each fluid the largest departure of $\delta\rho$ from zero and the density at which it occurs are listed:

fluid	NBP density, g/cm^3	$\delta\rho_{extreme}$, g/cm^3	$\rho_{extreme}$, g/cm^3
SF_6	1.35	0.0024	0.7
H_2O	0.96	0.0079	0.8
GeH_4	0.9	−0.0021	0.4

For a fluid as unusual as water, the maximum error in the density is 0.8% of the liquid density. We conclude that the errors in the densities of the refrigerants are probably no greater than 0.8% of their liquid densities. In particular, the critical densities, which are roughly 1/3 of the liquid densities, would be in error by 2.4% for fluids like water; however, the errors are almost certainly less.

The surface tensions computed from eq 1 depend upon $\rho_l - \rho_v$ at each temperature. If the present recipe for determining k near the boiling point and using it to compute $\rho_l - \rho_v$ were followed for water, the error in $\rho_l - \rho_v$ would be very small near the boiling point and would increase to 1.4% at $t = 0.01$. Thus, neglecting the variation of k leads to systematic errors in σ on the order of 1.4%.

Equations 5, 7, 11, and 12 are satisfactory representations of the refractive index data and the derived densities in the vicinity of the critical points. Indeed, they were used to determine ρ_c and T_c. However, these equations determine the vapor density as a difference between two quantities comparable to ρ_c. Thus these equations result in vapor densities with very large fractional errors and they should not be extrapolated to low temperatures.

VI. Comparison with Other Data

Higashi et al.[6] reported the critical temperature of R152a to be 386.44 ± 0.01 K; Mears et al.[4] reported 386.65 ± 0.5 K. Both results are consistent with the present value 386.35 ± 0.1 K. The data of Higashi et al. are concentrated within 10 K of T_c and are certainly more precise.

Higashi et al.[6] reported the critical density of R152a to be 368 ± 2 kg/mol; Mears et al.[4] reported 365 ± 10 kg/mol. We find 369 ± 9 kg/mol, where the error is dominated by possible deviations from the Lorentz–Lorenz relationship. The data of Mears et al. span the temperature range −41 to 80 °C. In that range they found $\rho_d = 1.042$, which is quite close to the value $\rho_d = 1.038$ that best fits the present data in the temperature range 23–111 °C.

For R142b, Mears et al.[4] report $T_c = 410.25 \pm 0.5$ K, $\rho_c = 435 \pm 10$ kg/m^3, and $\rho_d = 1.084$ in the temperature range −40 °C $< T <$ 126 °C. In the present work we find $T_c = 410.3 \pm 0.1$ K, $\rho_c = 449 \pm 11$ kg/m^3, and $\rho_d = 0.911$ in the temperature range −23 °C $< T <$ 136 °C. The values for ρ_c agree within their combined errors. The values for ρ_c and ρ_d are highly correlated.

(12) Maass, M.; Wright, C. H. *J. Am. Chem. Soc.* **1921**, *43*, 1098. Katz, D. L.; Saltmann, W. J. *Ind. Eng. Chem.* **1939**, *31*, 91.

(13) Schiebener, P.; J. Straub, J.; Levelt Sengers, J. M. H.; Gallagher, J. S. *J. Phys. Chem. Ref. Data* **1990**, *19*, 677.

(14) Balzarini, D.; Palffy, P. *Can. J. Phys.* **1974**, *52*, 2007.

(15) Palffy-Muhoray, P.; Balzarini, D. *Can. J. Phys.* **1978**, *56*, 1140.

Thus, the difference between the presents value and that from ref 4 reflects the differences between the values of ρ_c. For R142b, Valtz et al.[5] report T_c = 410.30 K without commenting on possible errors. Their value agrees with both the present value and the value from ref 4.

VII. Instability of R141b

Decomposition of R141b was evident in samples that had been exposed to the higher temperaures near T_c. The value of T_c finally listed in Table I was determined in a separate experiment. A fresh sample of R141b was loaded into the cell and the oil bath was heated to near T_c within 2 h. Two additional hours were required to observe the repeated disappearance and reappearance of the meniscus carefully enough to bracket T_c within ±0.040 K. Afterwards the cell and contents were maintained near T_c for 24 h. During this interval the contents of the cell became visibly discolored. The discoloration reduced the precision with which we were able to relocate T_c to ±0.5 K. Within this precision T_c had not changed from the previous determination.

The oil bath was allowed to cool overnight and the cell was then opened. A black residue coated all the surfaces that had been inside the cell. The crown glass prism had been most seriously affected and appeared to have been etched. The formerly high quality optical surfaces now scattered light significantly. The Pyrex capillary tubes did not appear to have been etched. In future measurements the crown glass prism will be replaced by a fused silica prism. The other materials with which the R141b came in contact (stainless steel, gold and sapphire) did not appear to have been affected.

The value of T_c determined in this separate experiment was 0.6 K below that determined by the refractive index data in a run that lasted 16 h. From this limited evidence, we conclude that the decomposition raises the apparent critical temperature. In this earlier run, the decomposition was not so strikingly visible. Nevertheless, the temperatures tabulated in Table IV for these earlier data were reduced by a linear function of time to account for the increase in the apparent critical temperature in a very approximate fashion.

Acknowledgment. We thank Graham Morrison and Dave Ward of NIST for providing us with density and vapor pressure data prior to their publication. Mark McLinden of NIST provided us with key references and a very helpful evaluation of density data. This work was sponsored, in part, by the U.S. Department of Energy, Office of Buildings and Community Systems, the American Society of Heating, Refrigerating and Air-Conditioning Engineers, and the U.S. Environmental Protection Agency, Global Change Division. We gratefully acknowledge the assistance of Helen Connan and Dorothy Harris of the DuPoint Co. in obtaining a sample of R152a, of Rajat Basu of Allied Signal Corp. in obtaining a sample of R123a, and of Richard Crooker of Pennwalt Corp. in obtaining a sample of R141b.

Registry No. R123a, 354-23-4; R141b, 1717-00-6; R134, 359-35-3; R142b, 75-68-3; R152a, 75-37-6.

Dynamic Studies of *s*-Trioxane in the Solid State and in Liquid Crystalline Solutions by Deuterium NMR

E. Gelerinter,† Z. Luz,* R. Poupko, and H. Zimmermann‡

The Weizmann Institute of Science, Rehovot 76100, Israel *(Received: March 27, 1990)*

Deuterium NMR is used to study dynamic processes involving perdeuterated *s*-trioxane in the solid state and in a liquid crystalline solution. In the solid state the *s*-trioxane molecules undergo threefold jumps about their C_3 symmetry axis. The rate of this process was measured in a powder solid sample between room temperature and the melting point (65 °C), yielding the rate equation $k_J = 2.35 \times 10^{18} \exp(-19.0/RT)$, where R is in kcal mol^{-1} K^{-1}. No indication of ring inversion in solid *s*-trioxane was found. In single crystals of *s*-trioxane a decrease in the signal intensity of the equatorial deuterons was detected below room temperature. The mechanism responsible for this loss in intensity remains an open question. In normal and liquid crystalline solutions *s*-trioxane undergoes chair–chair interconversion. The kinetic parameters for this reaction were determined by deuterium NMR in a solution of perdeuterated *s*-trioxane in a liquid crystalline solvent, yielding the rate equation $k = 1.5 \times 10^{14} \exp(-12.2/RT)$. It is demonstrated that by using 2D exchange spectroscopy the dynamic range over which this process can be investigated may be extended to much slower rates than those determined from line broadening.

Introduction

Proton NMR second moment and relaxation measurements indicate that in crystalline *s*-trioxane the molecules undergo thermally activated reorientation about their C_3 axes.[1-3] The quantitative interpretation of such measurements is, however, subject to considerable uncertainty because they require the separation of the measured effects into contributions from intra- and intermolecular dipolar interactions[4] and because the results are not always uniquely related to the mechanism of the dynamic process. For such studies, deuterium NMR seems more appropriate, since it reflects the local properties of the nuclei through their quadrupole interaction, thus providing more direct information concerning the dynamics in the various molecular sites.[5,6] Until recently, no such deuterium studies on trioxane (in the following we delete the prefix *s*- from *s*-trioxane) were possible because of its inavailability in a deuterated form. We have now succeeded in preparing perdeuterated trioxane (trioxane-d_6) by direct synthesis from deuterated paraformaldehyde and have already used it in a study of the urea-trioxane inclusion compound (UTIC).[7] Here we use this isotopic species to study the molecular

† Permanant address: Department of Physics and Liquid Crystal Institute, Kent State University, Kent, OH 44242.
‡ Permanent address: Max Planck Institut für Medizinische Forschung, AG Molekülkristalle, Jahnstrasse 29, D-6900 Heidelberg, FRG.

(1) Komaki, A.; Matsumoto, T. *Polym. Lett.* **1963**, *1*, 671.
(2) Slonim, Y.; Urman, Y. G.; Ermolaev, A. D. *Russ. J. Struct. Chem.* **1965**, *6*, 509.
(3) Resing, H. A.; Garroway, A. N. *Mol. Cryst. Liq. Cryst.* **1979**, *52*, 103.
(4) Slichter, C. P. *Principles of Magnetic Resonance*, 3rd ed.; Springer-Verlag; Berlin, 1989; Chapter 3.
(5) Schwartz, L. J.; Meirovitch, E.; Ripmeester, J. A.; Freed, J. H. *J. Phys. Chem.* **1983**, *87*, 4453.
(6) Vega, A. J.; Luz, Z. *J. Chem. Phys.* **1987**, *86*, 1803.
(7) Gelerinter, E.; Luz, Z.; Poupko, R.; Zimmermann, H. *J. Phys. Chem.* **1990**, *94*, 5391.

0022-3654/90/2094-8845$02.50/0